Auger decay of 4*d* inner-shell holes in atomic Hg leading to triple ionization

J. Andersson,[1] R. Beerwerth,[2,3] A. Hult Roos,[1] R. J. Squibb,[1] R. Singh,[1] S. Zagorodskikh,[4,1] O. Talaee,[1,5] D. Koulentianos,[1,6] J. H. D. Eland,[1,7] S. Fritzsche,[2,3] and R. Feifel[1,*]

[1]*Department of Physics, University of Gothenburg, Origovägen 6B, SE-412 58 Gothenburg, Sweden*

[2]*Helmholtz-Institute Jena, D-07743 Jena, Germany*

[3]*Theoretisch-Physikalisches Institut, Friedrich-Schiller-Universität Jena, D-07743 Jena, Germany*

[4]*Department of Physics and Astronomy, Uppsala University, Box 516, SE-751 20 Uppsala, Sweden*

[5]*Nano and Molecular Systems Research Unit, University of Oulu, P.O. Box 3000, FI-90014 University of Oulu, Finland*

[6]*Sorbonne Universités, UPMC Univ Paris 6, UMR7614, Laboratoire de Chimie Physique-Matière et Rayonnement, F-75005 Paris, France*

[7]*Department of Chemistry, Physical and Theoretical Chemistry Laboratory, Oxford University, South Parks Road, Oxford OX1 3QZ, United Kingdom*

(Received 21 April 2017; published 5 July 2017)

Formation of triply ionized states upon the creation of 4*d* inner-shell holes in atomic Hg is investigated by using synchrotron radiation of 730 eV photon energy and a versatile multielectron coincidence detection technique in combination with multiconfiguration Dirac-Fock calculations. By carefully selecting Coster-Kronig electrons detected only in coincidence with a 4*d* photoelectron, the Coster-Kronig spectrum has been extracted and the corresponding branching ratios of the 4*d* hole have been determined. The results are found to differ from previously established experimental ratios based on electron impact ionization but to agree now better with theory. We also present an Auger cascade analysis of pathways leading to triply ionized states of atomic Hg upon removal of a 4*d* inner-shell electron.

DOI: 10.1103/PhysRevA.96.012505

I. INTRODUCTION

Multielectron coincidence spectroscopy is an important method for studying electron correlations in atomic and molecular systems. To fully understand the nature of inner-shell hole induced Auger cascades, it is important to obtain information on all electrons emitted in the decay process. Kinetic-energy resolved coincident detection of several electrons can give information on the relations between all the different decay pathways in multiple ionization events. Such events typically involve emission of Auger electrons whose energies and intensities carry vital information on the decay pathways. From these pathways, the final charge state ratios can be estimated and the relaxation of the electron density that eventually cause molecular fragmentation and Coulomb explosions can be explained in detail [1–3].

Electron rearrangement is expected whenever an inner-shell vacancy is created. Depending on the shell structure of the electron hole state, single or multiple Auger decays leading to multiply charged states can be expected. To probe the electron correlations involved in Auger cascades, one must generally detect Auger electrons over a comparatively large kinetic-energy range at the same time. This is often a limiting factor for conventional electron spectroscopy techniques. However, the magnetic bottle technique [4] is highly efficient for coincidence studies as it collects essentially all electrons emitted in a solid angle of 4π and over a wide range of kinetic energies. The high collection efficiency of a magnetic bottle in combination with the high flux and energy resolution offered by synchrotron radiation sources makes a perfect match for studying Auger cascades following the creation of an inner-shell hole. Several examples of double and triple ionization studies of rare gas atoms using a magnetic bottle spectrometer have already been published [2,5–8]. These studies demonstrate the wealth of information that can be obtained from this kind of experiment. However, apart from some studies on, for instance, double and triple ionization of Cd [9,10] and studies on Auger decay pathways leading to multiply charged states in Hg [11–14] upon the formation of shallow inner-shell vacancies, the extent of studies on multiple ionization of metal atoms based on coincidence techniques is still very limited.

In this work, we present results on Auger cascades in metal atoms induced by inner-shell hole formation. In particular, we investigate triple ionization of atomic Hg upon creation of a 4*d* hole by using a magnetic bottle spectrometer and soft x-ray synchrotron radiation of primarily 730 eV photon energy. By carefully selecting Auger electrons detected in coincidence with a 4*d* photoelectron, candidate pathways for the main Auger channels leading to the experimentally observed Hg^{3+} final states are identified with the aid of multiconfiguration Dirac-Fock (MCDF) calculations. Furthermore, it has been shown that the decay of the 4*d* hole states is significantly influenced by the $4d^{-1} \rightarrow 4f^{-1}(nl)^{-1}$ Coster-Kronig (CK) process [15]. The CK process corresponds to an Auger process where the hole state is filled by an electron from a higher subshell with the same principal quantum number. These decay processes occur on very short time scales, sometimes causing large broadening (~25 eV; for comparison 1 eV corresponds to ~600 attoseconds) in the electron spectra [16]. As part of the Auger cascade analysis, we present a study of the $4d^{-1}$ Coster-Kronig (CK) process in Hg based on photoelectron-Auger electron coincidence measurements. This allows us to estimate the relative group intensities of the $4d^{-1} \rightarrow 4f^{-1}5d^{-1}$, $4d^{-1} \rightarrow 4f^{-1}5p^{-1}$, and $4d^{-1} \rightarrow$

*raimund.feifel@physics.gu.se

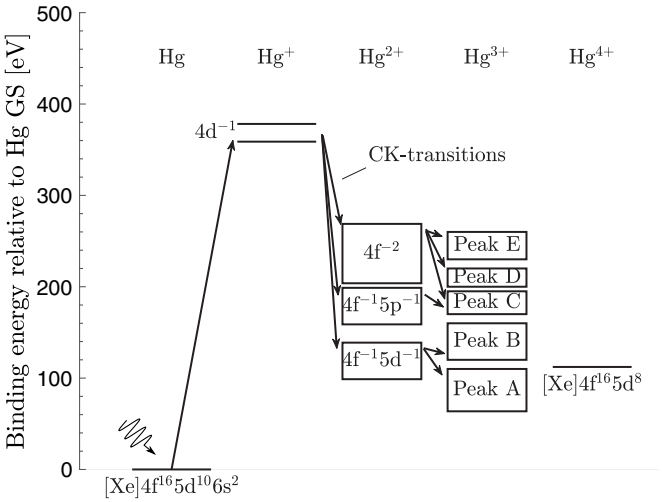

FIG. 1. Energy-level diagram of atomic Hg for different charge states. The arrows indicate possible transitions leading to the first three charge states. The level regions of Hg^{3+} are labeled based on spectral structures studied in subsequent figures.

$4f^{-2}$ CK transitions, schematically illustrated in Fig. 1, from coincidental detections of two, three, four, and five electrons associated with a single ionization event using primarily the photon energy of 730 eV, and 840 and 950 eV photons for cross-check purposes. These results are discussed and compared with previous theoretical and experimental results [15].

II. EXPERIMENT

The experiments were carried out at beamline U49/2-PGM-2 of the BESSY-II storage ring in Berlin, Germany. The storage ring was operated in single bunch mode at approximately 1.25 MHz repetition rate. To minimize the risk of detecting slow and fast electrons originating from different light pulses, the repetition rate was reduced further to about 78 kHz by a synchronized mechanical chopper [17]. This corresponds to a detection window for electron flight times up to about 12 μs, which is sufficiently long for extracting even the slowest electrons. To minimize the risk of several ionization events per light pulse, the radiation flux was adjusted to yield an electron count rate that implies a probability of an ionization event of less than $\sim$1% per light pulse. This makes single and multiple ionization events caused by a single photon distinguishable. In particular, it allows the selection of individual electrons involved in the formation of specific charge states and their correlations with other electron kinetic energies. Liquid Hg was evaporated using a thermostatically controlled oven similar to the device used in Ref. [18], heated to about 60 °C.

The magnetic bottle spectrometer [4] collects essentially all electrons emitted from an ionization event in the interaction volume by using a divergent magnetic field created by a $\sim$1 T strong permanent neodymium iron magnet. The divergent shape of this strong magnetic field is shaped by a soft iron conical pole piece to guide the electrons towards the about 2-m-long flight tube which is surrounded by a solenoid. The solenoid current of typically 1.5 A produces a weak, axial, homogeneous magnetic field that couples to the strong field, producing in this way the "bottleneck" shape of this spectrometer type. Inside the flight tube, the axial field guides the electrons on spiral trajectory towards a microchannel plate (MCP) detector located at the other end of the tube. The total collection-detection efficiency is about 50%–60% and is mainly limited by the detection efficiency of the MCP.

III. DATA ANALYSIS

The energies of the $4d$ hole states lie high up in the Hg^+ continuum, and are thus expected to decay efficiently into higher charge states by Auger decay (cf. Fig. 1). Our data show decays to Hg^{3+}, Hg^{4+}, and Hg^{5+}. A direct consequence of the 50%–60% collection-detection efficiency is that data sets of k-coincidentally recorded electrons can include electrons from ionization events producing higher charge states than Hg^{k+}. We call these "false" coincidences. Specifically, in the case of triple events these false coincidences may originate from ionization events releasing more than three electrons, but where only three were recorded. This can cause false patterns and confuse, for instance, the triple ionization spectrum. The influence of false coincidences from the production of n-fold ionized states in the data sets of k-coincidentally detected electrons relates to the binomial distribution

$$B(n,k,f_e) = \sum_{n>k} \binom{n}{k} f_e^k (1-f_e)^{n-k}, \qquad (1)$$

where f_e is the collection-detection efficiency, i.e., the probability of recording one electron. From tabulations of the ionization thresholds in Hg [19], the binding energy of a $4d$ hole in Hg^+ is less than the energy required to produce charge states higher than Hg^{7+}. Furthermore, a rough theoretical estimate of the charge-state production from the decay of a $4d$ hole suggests that about 1.1% leads to Hg^{2+}, 22% to Hg^{3+}, 55% to Hg^{4+}, and 22% to Hg^{n+}, where $5 \leqslant n \leqslant 7$. According to Eq. (1), the probability to detect a quadruple decay as a false triple decay is $B(4,3,f_e) \approx 0.25$–0.35. If we consider only the contribution of false triples from the charge-state production of Hg^{4+}, we expect about 16%–20% of the detected events in the triples data to belong to triply ionized states that do not decay further by Auger electron emission. False coincidences from events leading to higher charged states than Hg^{4+} are neglected due to our incomplete knowledge on the ion yields.

Many of the Auger pathways leading to Hg^{4+} are expected to go stepwise via the different charge states and thus also via Hg^{3+}. If the three recorded hits are the electrons emitted during the first three steps of the ionization process, the event should be interpreted as either the formation of a stable state in Hg^{3+} or as a snapshot of the cascade at the charge stage Hg^{3+} but where the system later relaxes further by either radiative transitions or Auger decay. Such false coincidences may cause intensity discrepancies between the calculated and experimental spectra. In contrast, if one (or more) of the three detected electrons comes from the fourth (or later) step in the ionization process, the event may cause false additional structures in the triples data when higher

charge states are energetically accessible. Effects from both of these mentioned scenarios are important to keep in mind for the results presented below.

IV. THEORY

We carried out calculations of the charge-state production, the population of the final states, and the electron spectra in order to provide guidance for interpreting the experimental data. Our computations assume sequential Auger decay of the inner-shell holes that are created by direct ionization of the 4d shells. This model is very similar to the one previously employed in Ref. [10]. Due to the large number of intermediate states we are unable to provide a thorough analysis of possible shake-up transitions as was done in Ref. [10].

We employ the MCDF method [20] to generate approximate wave functions and to compute the corresponding energy spectrum that is needed for our analysis. The wave function Ψ for a fine-structure level with parity P and total angular momentum J is represented as a superposition of N configuration state functions Φ (CSFs),

$$\Psi(\gamma, P, J) = \sum_{i=1}^{N} c_i(\gamma)\Phi(\gamma_i, P, J), \tag{2}$$

of the same P and J. The CSFs are jj-coupled superpositions of Slater determinants, which are uniquely specified by P, J, and a set of additional quantum numbers γ_i. The single-electron orbitals are variationally determined with a self-consistent procedure based on the Dirac-Coulomb Hamiltonian as implemented in the GRASP2K package [21]. The expansion coefficients $c_i(\gamma)$ are computed by the configuration interaction method [22] that solves the eigenvalue problem $H\mathbf{c} = E\mathbf{c}$, where $\mathbf{c}$ is the vector of the expansion coefficients and H is the Hamiltonian.

Once the wave functions are obtained for all three charge states under consideration, we utilize the RATIP package [23] to compute the photoionization cross sections and Auger transition rates. For the photoionization of neutral Hg, the PHOTO component of RATIP is utilized to compute the cross section σ_{ij} for ionizing the ground level i of neutral Hg to a hole state j in Hg^+, that is subsequently used to compute the relative population P_{ij} of Hg^+. In the next step, the Auger decay rates $\Gamma_{j\to k}$ of these autoionizing states to the fine-structure levels k of Hg^{2+} are computed for all energetically allowed transitions using the AUGER component of RATIP. These rates are again combined to obtain the branching ratio of a decay from fine-structure level j in Hg^+ to level k in Hg^{2+} as given by $P_{jk} = \Gamma_{j\to k}/\sum_n \Gamma_{j\to n}$. Similarly, the branching ratios P_{kl} for the second Auger decay from Hg^{2+} to Hg^{3+} are computed. These branching ratios are found to be less sensitive to uncertainties due to neglected electron correlation contributions than the absolute transition rates.

In the next step, these decay probabilities are combined to the total probability of a specific decay path that consists of the photoionization followed by two sequential Auger decays, as $P_{ij}P_{jk}P_{kl}$. These transition probabilities include, in principle, all information about the occurring decay processes. However, the wealth of information is too sophisticated for a detailed comparison with experimental data, such that further processing of the computed data is necessary. In this model, we also neglect direct double Auger processes that are a higher-order process and thus weak, as well as radiative losses due to fluorescence.

The energy spectrum of the emitted Auger electrons can be obtained when the analysis is restricted to one or a range of final levels l. The resulting set of possible decay paths from the neutral initial state i to the triply charged final state l and their corresponding probabilities allows one to compute electron spectra from known transition energies. In order to account for experimental and lifetime broadenings, the computed spectra are convoluted with a Voigt profile. The Gaussian broadening σ is chosen to resemble the experimental resolution and the Lorentzian broadening γ is set by the computed Auger transition rates. In the latter case, γ is given by the sum of the total decay width of the initial and final level $\gamma = \Gamma_i + \Gamma_f$. For the electron spectra that arise in the formation of the low-lying final states of Hg^{3+} this yields very good agreement with the measured spectra, while for the higher-lying final states (above the ionization threshold for Hg^{4+}) the agreement is rather qualitative. In this region, we often observe large uncertainties in the computed energies. This could affect the computed transition rates if the calculated pathways include some energetically forbidden decays or, conversely, exclude some decays that are actually allowed.

When the probabilities are summed over all intermediate states j and k, one obtains the relative population of a final state l as $P_l = \sum_{j,k} P_{ij}P_{jk}P_{kl}$. A final-state spectrum (see, e.g., Fig. 4 below) is obtained by repeating this for all fine-structure levels of Hg^{3+}. When these population probabilities are again summed over all fine-structure levels of one charge state that lie below the ionization threshold of the next higher charge state, an estimate for the charge-state production can be obtained, for example, for Hg^{3+} as $\mathrm{Br}(Hg^{3+}) = \sum_l P_l = \sum_{j,k,l} P_{ij}P_{jk}P_{kl}$.

For the wave functions generated in this work, we included all electron configurations into the expansion (2) that arise in the two-electron Auger decay of the 4d hole configuration. In addition, the higher-lying holes $5s^{-1}$, $4f^{-1}$, $5p^{-1}$, $5d^{-1}$, and $6s^{-1}$ were included into the first ionization stage as they have been found to influence the CK branching ratios in the first Auger decay by configuration interaction. Therefore, our wave functions are superpositions of 1 CSF for the ground state of Hg, 10 CSFs for Hg^+, 99 CSFs for Hg^{2+}, and 578 CSFs for Hg^{3+}. These expansions of the wave function give rise to a total of ~306 and ~15 100 transitions for the first and second Auger step, respectively. The next higher charge state Hg^{4+} would involve a total of about 2900 CSFs (fine-structure levels), giving rise to another ~160 000 Auger transitions. These numbers increase even further for the Auger decay to Hg^{5+} making the computations of these high charge states extremely demanding. Furthermore, the number of intermediate configurations would exponentially grow when shake-up transitions are included, which is the primary reason why they are mostly omitted in the present work. That is, only transitions between already occupied configurations are considered, but not additional valence shake-up states of the form $6s \to 7s$ and $6s \to 6p$ as in Ref. [10].

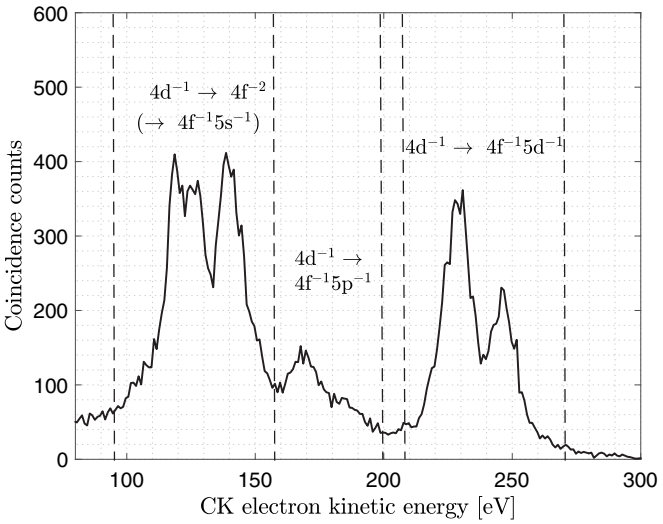

FIG. 2. Coster-Kronig spectrum associated with the decay of the $4d^{-1}$ states in atomic Hg. Three regions representing the decay into mainly three different double hole configurations are marked. The leftmost region shows predominantly decays to $4f^{-2}$, the middle region to $4f^{-1}5p^{-1}$, and the rightmost region to $4f^{-1}5d^{-1}$.

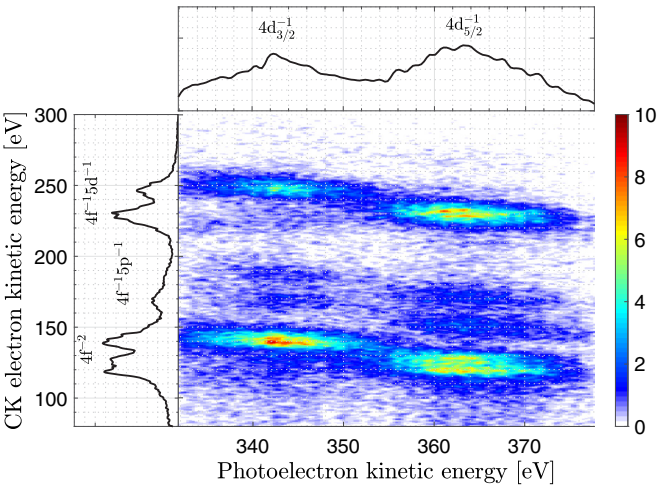

FIG. 3. Coincidence map reflecting the correlations of $4d$ photoelectrons (horizontal axis) and Coster-Kronig electrons (vertical axis). To highlight features in the map, a Gaussian smoothing filter has been applied to each bin of the two-dimensional histogram. Intensity projections of the coincidence map onto the horizontal and vertical axis show the photoelectron spectrum and the Coster-Kronig spectrum, respectively.

V. RESULTS

A. Coster-Kronig decay of 4*d* hole states

According to previous studies of free Hg atoms [15], the $4d$ holes are expected to decay mainly by CK transitions of the type $4d^{-1} \rightarrow 4f^{-2}$, $4d^{-1} \rightarrow 4f^{-1}5p^{-1}$, and $4d^{-1} \rightarrow 4f^{-1}5d^{-1}$, as illustrated in Fig. 1. An experimental CK spectrum obtained at the photon energy of 730 eV is presented in Fig. 2. The three main groups of CK transitions are labeled in this figure accordingly. To minimize the risk of including shake-up transitions in the analysis, the coincidences were limited to include only electrons that were measured in coincidence with a $4d$ photoelectron falling within one FWHM of a pseudo-Voigt profile fitted to the $4d$ photoelectron lines. The general structure of the CK spectrum resembles those previously measured by Aksela *et al.* [15] on free Hg atoms as well as measurements by Matthew *et al.* [24] on the three adjacent elements Ir, Pt, and Au in condensed form. These studies have shown interesting discrepancies as compared with predicted relative intensities between the CK groups. The relative intensities derived experimentally by Aksela *et al.* suggested the $4f^{-1}5d^{-1}$ group intensity to be stronger than that of the $4f^{-2}$ group by about 14%–40%, while the results of Matthew *et al.* showed an opposite relationship with the $4f^{-2}$ group being 50% stronger than the $4f^{-1}5d^{-1}$ group.

This contradiction between the measured and theoretical ratios motivated us to estimate the ratios once more but with a different method. To minimize effects due to differences in photon energies and potential overlap of photoelectron and Auger electron lines from, e.g., $4p^{-1} \rightarrow (nl)^{-1}(n'l')^{-1}$ transitions, we based our estimates on measurements done at three different photon energies, specifically 730, 840, and 950 eV. After selecting coincidence events as explained above, the data were examined in the form of two-dimensional histograms, henceforth referred to as coincidence maps. Figure 3 shows a coincidence map obtained at the photon energy of 730 eV. This map represents the distribution of correlations between the kinetic energies of a $4d$ photoelectron (x axis) and a CK electron (y axis), with a linear color scale representing the relative counts of coincidence events. To estimate the relative intensity of the CK transitions, the intensities of the relevant islands in the map were integrated for each photon energy. The same procedure was performed for all the data sets of double, triple, quadruple, and quintuple events to reduce the risk of an integration bias caused by the 50%–60% collection-detection efficiency. Table I lists the intensity ratios based on all photon energies together with one standard deviation.

The results are substantially different from those of Aksela *et al.* [15] but agree better with the ratios of related transitions in Ir, Pt, and Au measured by Matthew *et al.* [24]. As already pointed out in Ref. [15], their discrepancy from the results of Matthew *et al.* could be attributed to a complicated background subtraction method and a varying collection efficiency of their spectrometer over the region of the CK electron kinetic energies. Another possible source of discrepancy could be related to the use of comparatively high electron impact energies (~3 keV). Ionization of deeper shells could lead to a biased population of the $4d$ hole

TABLE I. Intensity ratios of the $4d^{-1}$ CK groups presented as averages with one standard deviation based on three data sets obtained at the photon energies 730, 840, and 950 eV. Estimates on the theoretical uncertainty are based on the deviation between the different models.

Charge state	Expt. (%)	Theory (%)	Transition
Hg+	29.17 ± 0.96	30 ± 6	$4d^{-1} \rightarrow 4f^{-1}5d^{-1}$
	17.75 ± 0.51	26 ± 6	$4d^{-1} \rightarrow 4f^{-1}5p^{-1}$
	53.08 ± 1.11	32 ± 6	$4d^{-1} \rightarrow 4f^{-2}$
		12 ± 3	$4d^{-1} \rightarrow 4f^{-1}5s^{-1}$

states from decays of, for instance, $4p$ hole states by x-ray fluorescence. Such bias is not present in our data as we limit our data analysis to include only electrons which were measured in coincidence with an identified $4d$ photoelectron. As our $4d$ photoelectron coincidence measurements enable us to expand the data into two dimensions, the possibility of including background and population from deeper holes is significantly reduced. A previous work based on data recorded during the same experimental run time using the same experimental setup have also shown that the collection efficiency of our coincidence spectrometer does not vary significantly over the CK electron kinetic-energy region [25]. The experimental $4d^{-1} \rightarrow 4f^{-1}5d^{-1}$ group intensity agrees well with the calculations, while $4d^{-1} \rightarrow 4f^{-1}5p^{-1}$ and $4d^{-1} \rightarrow 4f^{-2}$ deviate more. According to our calculations, the $4f^{-1}5p^{-1}$ group is by far the most short lived of the three groups. This can be understood in terms of the spatial extent of the radial wave functions. Neither a $4f$ or a $5d$ hole can be filled by an electron from within the same n shell. However, a $5p$ hole can be filled by a $5d$ electron, leaving the $4f$ hole as a spectator in a rapid $4f^{-1}5p^{-1} \rightarrow 4f^{-1}5d^{-2}$ decay. The large broadening from this decay is expected to cause overlap with the $4f^{-2}$ group, leading to uncertain relative intensities between these two CK groups. In addition, the $4f^{-1}5s^{-1}$ group is expected to overlap strongly with the $4f^{-2}$ group and should according to our calculations account for approximately $1/3$ of the integrated intensity over the $4f^{-2}$ region. However, the theoretical branching ratios depend heavily on the details of the wave functions, which leads to rather large fluctuations in the relative intensity of the CK groups. Nevertheless, the $\sim 1/3$ ratio between the $4f^{-1}5s^{-1}$ group and the $4f^{-2}$ group remain relatively stable.

B. Formation of Hg^{3+} states

The two-hole states formed upon decay of the $4d$ holes still reside rather high up in the Hg^{2+} continuum and are thus expected to decay further by Auger electron emission. To study the decay of the two-hole states leading to Hg^{3+}, we formed a final-state histogram of the kinetic energies of three electrons detected in coincidence, selecting again on the $4d$ photoelectrons. This histogram, displayed in Fig. 4, represents a final-state spectrum based on triple coincidence counts per triple ionization potential (TIP). Here,

$$\mathrm{TIP} = h\nu - (\varepsilon_1 + \varepsilon_2 + \varepsilon_3), \tag{3}$$

where ε_i are the kinetic energies of the three electrons, and $h\nu$ the photon energy, which was 730 eV. The spectrum shows the relative population of the final states in Hg^{3+} upon decay of a $4d$ hole state. The Hg^{3+} ground state is expected to be located at TIP = 63.65 eV and the ground state of Hg^{4+} at 112.20 eV [19] above the ground state of neutral Hg. The spectrum in Fig. 4 shows five main features where only the first feature is energetically forbidden to decay into higher charge states. The experimental peak positions and assigned configurations are given in Table II. The positions of each feature were estimated by least-square fits of pseudo-Voigt profiles to the data by assuming a linear background. For comparison, a theoretical spectrum generated by simulating the two-step Auger cascades based on MCDF theory has been superimposed. The theoretical final-state spectrum was broadened with Gaussians of 1 eV width and the intensities were normalized to match peak A in the experimental spectrum. The candidate configurations for the five main features found with aid of these calculations are presented in Table II. It should be noted, however, that the labeled configurations are not the only configurations available at these energies. Auger pathways leading to different configurations at these energies are allowed but they are not significantly populated according to our calculations. Approximately 90% of the intensity of peak A is expected to be from transitions to the $5d^{-3}$ states. The lack of observable pathways leading to final-state configurations based on $6s$ holes, such as the $5d^{-1}6s^{-2}$ ground-state configuration of Hg^{3+}, is thought to be related to small orbital overlaps and low statistical weight for $4f^{-1} \rightarrow 6s^{-1}$ transitions compared to, e.g., the $4f^{-1} \rightarrow 5d^{-1}$ transitions.

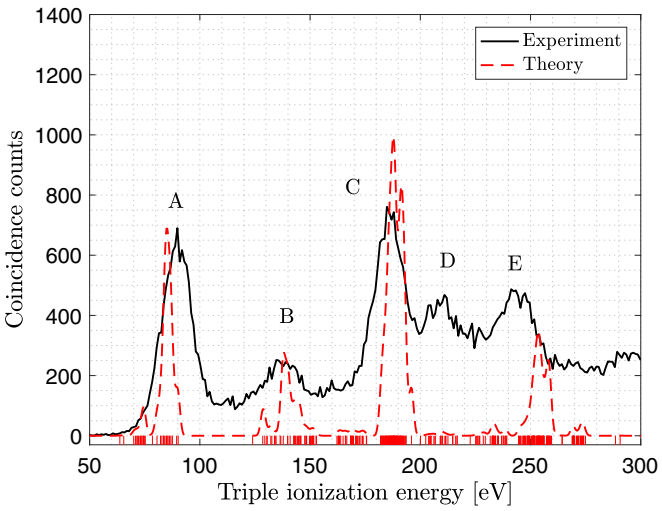

FIG. 4. Experimental spectrum of Hg^{3+} produced by ionization of $4d$ electrons using 730 eV photons and subsequent emission of two Auger electrons. The red dashed curve represents a theoretical final-state spectrum based on MCDF calculations of Auger cascades leading to Hg^{3+}.

As can be seen in Fig. 4, the theoretical spectrum agrees well with peaks A, B, C, and E, while it apparently does not populate states located at the position of peak D. The energies of these highly excited states are uncertain, which explains the shift in the position of peak E. Tests with differently optimized wave functions show that the population of peak B is very model dependent, while A, D, and E show more consistent results. This could be due to the large contribution of low-energy transitions that cannot be computed accurately due to a lack of precise spectral information. According to the calculated energy states, peak D could be associated with either the configuration $5s^{-1}5d^{-2}$ or $5p^{-2}5d^{-1}$ or with both of them. To investigate further how these states are possibly populated, we expanded the triple ionization spectrum into a two-dimensional coincidence map displayed in Fig. 5. In this figure, the horizontal axis shows the triple ionization spectrum, and the vertical axis shows the kinetic energies of the (two) Auger electrons measured in coincidence with a $4d$ photoelectron, which are involved in the formation of each final

TABLE II. Auger cascade pathways of the $4d$ hole states leading to triply ionized states in atomic Hg. The pathways were identified by comparison of the experimental data to the MCDF calculations. The labels in column 2 refer to the notations used in Figs. 6 and 7 and the positions in column 5 to the final-state peaks in Fig. 4. Column 4 presents within parentheses calculated relative intensities for some of the lines.

Peak	Label	Initial config.	Final config.	Position (eV)
A	1	$5p_{3/2}^{-1}5d^{-1}$	$5d^{-3}$	90.7
	2	$5p_{1/2}^{-1}5d^{-1}$	$5d^{-3}$	
	3	$4f^{-1}5d^{-1}$	$5d^{-3}$ (94%)	
		$4f^{-1}\,6s^{-1}$	$5d^{-2}6s^{-1}$ (6%)	
	4	$4f^{-1}5d^{-1}$	$5d^{-2}6s^{-1}$	
	5	$4d_{5/2}^{-1}$	$4f^{-1}5d^{-1}$	
	6	$4d_{3/2}^{-1}$	$4f^{-1}5d^{-1}$ (85%)	
		$4d_{5/2}^{-1}$	$4f^{-1}6s^{-1}$ (8%)	
		$4d_{5/2}^{-1}$	$5p^{-1}5d^{-1}$ (7%)	
	7	$4d^{-1}$	$5p^{-1}5d^{-1}$ (80%)	
		$4d_{3/2}^{-1}$	$4f^{-1}6s^{-1}$ (20%)	
	8	$4d_{3/2}^{-1}$	$5p^{-1}5d^{-1}$	
B	1	$4f^{-1}5d^{-1}$	$5p^{-1}5d^{-2}$	138.2
	2	$4f^{-1}5d^{-1}$	$5p^{-1}5d^{-1}6s^{-1}$	
	3	$4d_{5/2}^{-1}$	$5s^{-1}5d^{-1}$	
	4	$4d_{5/2}^{-1}$	$4f^{-1}5d^{-1}$	
	5	$4d_{3/2}^{-1}$	$4f^{-1}5d^{-1}$	
C	1	$4f^{-1}5p_{3/2}^{-1}$	$4f^{-1}5d^{-2}$	186.7
	2	$4f^{-1}5p_{1/2}^{-1}$	$4f^{-1}5d^{-2}$	
	3	$4f^{-2}$	$4f^{-1}5d^{-2}$	
	4	$4d^{-1}$	$4f^{-2}$	
	5	$4d^{-1}$	$4f^{-1}5p^{-1}$	
D	1	$5s^{-1}5p^{-1}$	$5s^{-1}5d^{-2}$	210.5
	2	$4f^{-2}$	$5s^{-1}5d^{-2}$	
		$4f^{-2}$	$5p^{-2}5d^{-1}$	
	3	$4d^{-1}$	$4f^{-1}5s^{-1}$	
		$4d^{-1}$	$4f^{-2}$	
	4	$4d^{-1}$	$4f^{-2}$	
		$4d^{-1}$	$5s^{-1}5p^{-1}$	
	5	$4d^{-1}$	$5s^{-1}5p^{-1}$	
E	1	$4f^{-1}5s^{-1}$	$4f^{-1}5p^{-1}5d^{-1}$ (43%)	245.0
			$4f^{-1}5p^{-1}6s^{-1}$ (15%)	
		$4f^{-2}$	$4f^{-1}5p^{-1}5d^{-1}$ (36%)	
			$4f^{-1}5p^{-1}6s^{-1}$ (6%)	
	2	$4d_{5/2}^{-1}$	$4f^{-2}$ (63%)	
		$4d_{5/2}^{-1}$	$4f^{-1}5s^{-1}$ (37%)	
	3	$4d_{3/2}^{-1}$	$4f^{-2}$ (51%)	
		$4d_{3/2}^{-1}$	$4f^{-1}5s^{-1}$ (49%)	

state. As seen in Fig. 5, only the peaks A and B in the triple ionization spectrum can be associated with the decay of the $4f^{-1}5d^{-1}$ states, which is in line with theoretical calculations. The formation of peak C seems to be associated with the decay of states associated with two intermediate double hole configurations, namely $4f^{-1}5p^{-1}$ and $4f^{-2}$. Peaks D and E are both associated with structures at energies similar to the $4f^{-2}$ states. The identified candidate pathways leading to the five final states are also given in Table II.

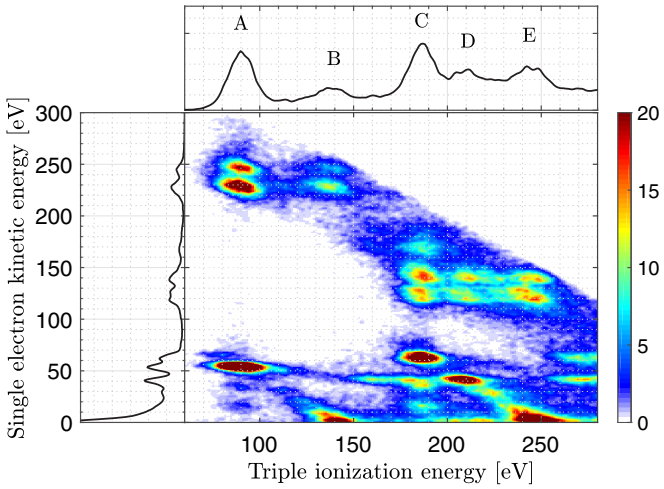

FIG. 5. Map of single Auger electrons (vertical axis) measured in coincidence with selected $4d$ photoelectrons and presented with the corresponding triple ionization final states (horizontal axis). A Gaussian smoothing filter has been applied to each bin of the two-dimensional histogram to highlight features present in that map.

C. Final-state peaks A and B

By selecting the electrons involved in the formation of the two lowest final state peaks A and B in Fig. 4, two corresponding single electron spectra based on the two Auger electrons emitted in the decay of the $4d$ hole states was extracted. These two experimental spectra are presented in Fig. 6 together with our simulated spectra. The peak labels are

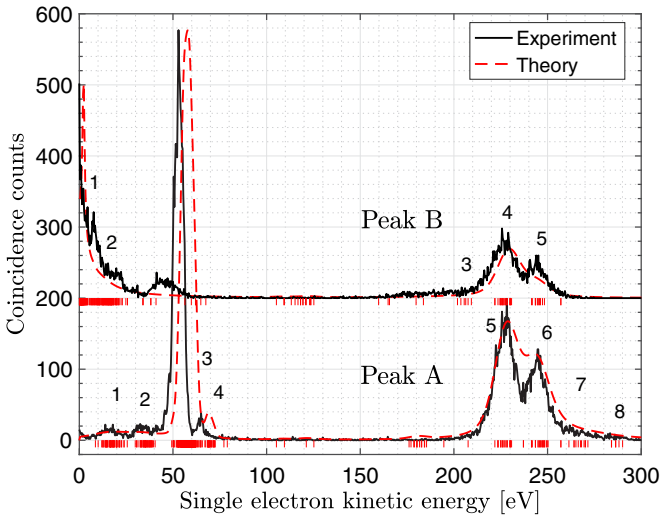

FIG. 6. Comparison of experimental and theoretical single-electron spectra associated with the two Auger electron kinetic-energy ranges producing peaks A and B in Fig. 4. The solid black curves display the experimental kinetic energies detected in coincidence with both a $4d$ photoelectron and a triple ionization energy corresponding to peaks A and B in Fig. 4, respectively. The red, dashed curves denote the simulated spectra with arbitrarily normalized intensities and a broadening using a Voigt profile based on the corresponding lifetime width and experimental resolution. The labeled peaks refer to the calculated positions of the transitions presented in Table II.

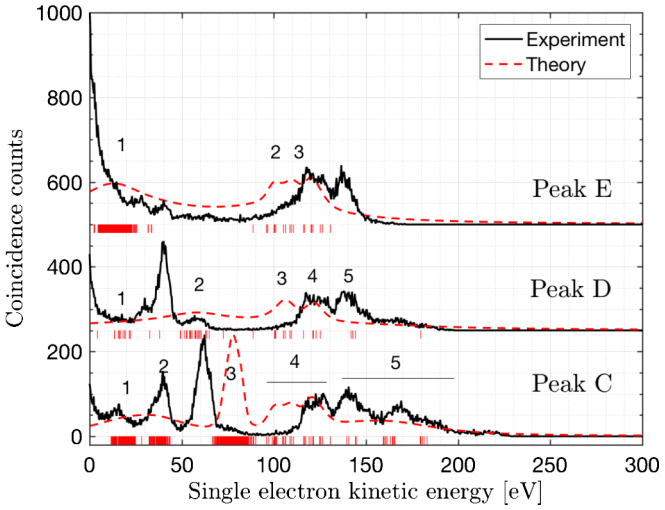

FIG. 7. Same as Fig. 6 but for the formation of peaks C, D, and E in Fig. 4. The solid black curves display the experimental kinetic energies detected in coincidence with a 4*d* photoelectron and which comply with the triple ionization energies of peaks C, D, and peak E, respectively. The red, dashed curves correspond to the simulated spectra with similar normalization and broadening procedure as in Fig. 6. The labeled peaks refer to the calculated positions of the transitions presented in Table II.

based on the calculated spectra and summarized in Table II. The calculated line intensities were broadened with a Voigt profile, defined by a Lorentzian width set by the calculated transition rates and a Gaussian width set by the experimental energy resolution, which follows approximately $\Delta\varepsilon \sim \varepsilon/50$. Generally, the theoretical results seem to agree fairly well with the experimental kinetic energies in the two single-electron spectra, but the experimental spectrum of single electrons involved in the formation of final-state peak B shows a structure at about 40–50 eV, which is not reproduced in the theoretical spectrum. This feature could be an artifact that is caused by overlapping electrons involved in the formation of final-state peak A (see Fig. 5).

The agreement between the experimental and theoretical spectra in Fig. 6 and of peaks A and B in Fig. 4 suggests that the possible contribution of false coincidences from events producing higher charge states is still negligible. This conclusion is further supported by a brief analysis of the experimental quadruple data where the counts in the $4d^{-1} \rightarrow 4f^{-1}5d^{-1}$ CK group are significantly fewer compared to the counts in the $4d^{-1} \rightarrow 4f^{-2}$ group.

D. Final-state peaks C, D, and E

The Auger cascades that lead to the peaks C, D, and E all involve the decay of the $4f^{-2}$ states. In addition, the decay of the $4f^{-1}5p^{-1}$ states also contribute to peak C, but less prominently. Figure 7 presents the single-electron spectra associated with each of the three final-state peaks. The agreement with theory is seemingly worse than for those of final-state peaks A and B. The primary reason for this relates to the uncertainty in the computed energy levels which is considerable for these highly excited states. The $4f^{-2}$ group is shifted toward lower energies, which leads to higher energies for the correlated transitions labeled as 3 in the formation of peak C in Fig. 7. A possible consequence of the shift in the computed energies is that the strong transitions leading to final-state peak D could become energetically forbidden. Specialized computations optimizing the highly excited part of the energy spectrum could circumvent this problem, but this will inevitably degrade the spectra associated with final-state peaks A and B.

Furthermore, it is clear from the quadruple coincidence data that a significant portion of the $4f^{-2}$ states decays further to at least Hg^{4+}. Therefore, the states associated with the peaks C, D, and E decay likely by further Auger electron emission. However, if a large portion of the $4f^{-2}$ states is expected to lead to Hg^{4+}, it is likely that a false final-state peak appears in the triple ionization spectrum consisting of the combination of a 4*d* photoelectron, a $4d^{-1} \rightarrow 4f^{-2}$ CK electron, and the last of the remaining two Auger electrons. This could also explain why peak D appears in the experimental triple ionization spectrum but is completely absent in our theoretical spectrum.

VI. CONCLUSIONS

Triple ionization electron coincidence data of atomic Hg upon decay of 4*d* inner-shell holes have been obtained using a magnetic bottle spectrometer and synchrotron radiation at the photon energies 730 eV, 840 eV, and 950 eV. Auger cascades of the 4*d* hole states were traced by the use of correlation analysis of electron kinetic energies measured in coincidence and with support of multiconfiguration Dirac-Fock calculations. Branching ratios of the $4d^{-1}$ Coster-Kronig decay groups were obtained and compared to previous theoretical and experimental works, where we find our results to be in much better agreement with theory. The coincidence detection technique applied in the present work removes possible population bias of the 4*d* holes and significantly reduces integrated background noise that could have possibly plagued previous conventional spectroscopic data. The second step of the Auger cascade has been interpreted by comparison to calculated Auger cascades resulting in the identification of several candidate pathways. The results presented here are expected to be of considerable interest for future studies on, for instance, Coulomb explosion of Hg-containing molecular systems or clusters.

ACKNOWLEDGMENTS

This work has been financially supported by the Swedish Research Council (VR) and the Knut and Alice Wallenberg Foundation, Sweden. We thank the Helmholtz Zentrum Berlin for the allocation of synchrotron radiation beam time. The research leading to these results has received funding from the European Community's Seventh Framework Programme (FP7/2007-2013) under Grant Agreement No. 312284. We would also like to warmly acknowledge the staff and colleagues at the Helmholtz Centre for Materials and Energy GmbH BESSY II, Berlin. This work has been funded in part by the German Federal Ministry for Education and Research (BMBF) under Grant Agreement No. 05K16SJA.

[1] T. A. Carlsson and R. M. White, Measurement of the relative abundances and recoil energy spectra of fragment ions produced as the initial consequences of x-ray interaction with C_2H_5I, CH_3CD_2I, and $Pb(CH_3)_4$, J. Chem. Phys. **48**, 5191 (1968).

[2] Y. Hikosaka, P. Lablanquie, F. Penent, T. Kaneyasu, E. Shigemasa, J. H. D. Eland, T. Aoto, and K. Ito, Single, double, and triple Auger decay of the Xe 4p core-hole states, Phys. Rev. A **76**, 032708 (2007).

[3] J. H. D. Eland, C. Slater, S. Zagorodskikh, R. Singh, J. Andersson, A. Hult-Roos, A. Lauer, R. J. Squibb, and R. Feifel, Ion charge-resolved branching in decay of inner shell holes in Xe up to 1200 eV, J. Phys. B **48**, 205001 (2015).

[4] J. H. D. Eland, O. Vieuxmaire, T. Kinugawa, P. Lablanquie, R. I. Hall, and F. Penent, Complete Two-Electron Spectra in Double Photoionization: The Rare Gases Ar, Kr, and Xe, Phys. Rev. Lett. **90**, 053003 (2003).

[5] E. Andersson, P. Linusson, S. Fritzsche, L. Hedin, J. H. D. Eland, L. Karlsson, J. E. Rubensson, and R. Feifel, Formation of Kr^{3+} via core-valence doubly ionized intermediate states, Phys. Rev. A **85**, 032502 (2012).

[6] P. Linusson, S. Fritzsche, J. H. D. Eland, M. Mucke, and R. Feifel, Single-photon multiple ionization forming double vacancies in the $2p$ subshell of argon, Phys. Rev. A **87**, 043409 (2013).

[7] P. Linusson, L. Hedin, J. H. D. Eland, R. J. Squibb, M. Mucke, S. Zagorodskikh, L. Karlsson, and R. Feifel, Complete double valence photoionization study of the electron spectra of krypton, Phys. Rev. A **88**, 022510 (2013).

[8] J. Palaudoux, P. Lablanquie, L. Andric, K. Ito, E. Shigemasa, J. H. D. Eland, V. Jonauskas, S. Kučas, R. Karazija, and F. Penent, Multielectron spectroscopy: Auger decays of the krypton 3d hole, Phys. Rev. A **82**, 043419 (2010).

[9] P. Linusson, S. Fritzsche, J. H. D. Eland, L. Hedin, L. Karlsson, and R. Feifel, Double ionization of atomic cadmium, Phys. Rev. A **83**, 023424 (2011).

[10] J. Andersson, R. Beerwerth, P. Linusson, J. H. D. Eland, V. Zhaunerchyk, S. Fritzsche, and R. Feifel, Triple ionization of atomic Cd involving $4p^{-1}$ and $4s^{-1}$ inner-shell holes, Phys. Rev. A **92**, 023414 (2015).

[11] J. Palaudoux, S.-M. Huttula, M. Huttula, F. Penent, L. Andric, and P. Lablanquie, Auger decay paths of mercury $5p$ and $4f$ vacancies revealed by multielectron spectroscopy, Phys. Rev. A **91**, 012513 (2015).

[12] S.-M. Huttula, J. Soronen, M. Huttula, F. Penent, J. Palaudoux, L. Andric, and P. Lablanquie, Auger decay of core valence double photoionized states in atomic mercury, J. Phys. B **48**, 115001 (2015).

[13] M. Huttula, S.-M. Huttula, P. Lablanquie, J. Palaudoux, L. Andric, J. H. D. Eland, and F. Penent, Spectroscopy of triply and quadruply ionized states of mercury, Phys. Rev. A **83**, 032510 (2011).

[14] M. Huttula, S.-M. Huttula, S. Fritzsche, P. Lablanquie, F. Penent, J. Palaudoux, and L. Andric, Core-valence double photoionization of atomic mercury, Phys. Rev. A **89**, 013411 (2014).

[15] H. Aksela and S. Aksela, $N_{4,5}N_{6,7}X$ Coster-Kronig spectra of free Hg atoms, J. Phys. B **16**, 1531 (1983).

[16] M. Ohno, Strong dynamical effects in the x-ray photoemission spectra and x-ray emission spectra of the elements Pd to Xe, Phys. Scr. **21**, 589 (1980).

[17] S. Plogmaker, P. Linusson, J. H. D. Eland, N. Baker, E. M. J. Johansson, H. Rensmo, R. Feifel, and H. Siegbahn, Versatile high-repetition-rate phase-locked chopper system for fast timing experiments in the vacuum ultraviolet and x-ray spectral region, Rev. Sci. Instrum. **83**, 013115 (2012).

[18] J. H. D. Eland, R. Feifel, and D. Edvardsson, Single and double photoelectron spectroscopy of atomic mercury, J. Phys. Chem. A **108**, 9721 (2004).

[19] A. Kramida, Yu. Ralchenko, and J. Reader, NIST Atomic Spectra Database, available at http://physics.nist.gov/asd.

[20] I. P. Grant, *Relativistic Quantum Theory of Atoms and Molecules: Theory and Computation* (Springer Science & Business Media, New York, 2007), Vol. 40.

[21] P. Jönsson, X. He, C. Froese Fischer, and I. P. Grant, The grasp2K relativistic atomic structure package, Comput. Phys. Commun. **177**, 597 (2007).

[22] S. Fritzsche, C. Froese Fischer, and G. Gaigalas, RELCI: A program for relativistic configuration interaction, Comput. Phys. Commun. **148**, 103 (2002).

[23] S. Fritzsche, The Ratip program for relativistic calculations of atomic transition, ionization, and recombination properties, Comput. Phys. Commun. **183**, 1525 (2012).

[24] J. A. D. Matthew, F. P. Netzer, and E. Bertel, The $N_{4,5}N_{6,7}N_{6,7}$ and $N_{4,5}N_{6,7}O_{4,5}$ Auger spectra of Au, Pt and Ir, J. Electron Spectrosc. Relat. Phenom. **20**, 1 (1980).

[25] A. Hult Roos, J. H. D. Eland, J. Andersson, S. Zagorodskikh, R. Singh, R. J. Squibb, and R. Feifel, Relative extent of double and single Auger decay in molecules containing C, N and O atoms, Phys. Chem. Chem. Phys. **18**, 25705 (2016).